ImmunoTargets and Therapy

Dovepress
Taylor & Francis Group

Open Access Full Text Article

ORIGINAL RESEARCH

Enhancing Anti-CTLA-4 Antibody Delivery to the Brain Using Focused Ultrasound and Microbubbles

Maria Afonso Pereira[1], Vanessa Drevenakova[1,2], Qiyixing Ethan Liu[1], Sarina Grewal[1–3], Sophie V Morse[1,2]

[1]Department of Bioengineering, Imperial College London, London, UK; [2]UK Dementia Research Institute Centre, Imperial College London, London, UK; [3]Department of Brain Sciences, Imperial College London, London, UK

Correspondence: Sophie V Morse, Department of Bioengineering, Imperial College London, London, UK, Email sophie.morse11@imperial.ac.uk

Introduction: Gliomas, particularly glioblastomas, are characterised by their poor prognosis and low patient survival rate. Cytotoxic T lymphocyte-associated antigen-4 antibodies, a type of immune checkpoint inhibitor, have shown promise as an effective treatment strategy against the most aggressive tumour cells within the microenvironment of gliomas. However, their delivery to the brain is hindered by the blood-brain barrier, which is leaky in a heterogenous way, leading to uneven drug distribution across the tumour. Focused ultrasound, combined with intravenously administered microbubbles, is a technique that can non-invasively, safely, and reversibly increase the permeability of the blood-brain barrier in a targeted area, promoting the delivery of therapeutics, such as immune checkpoint inhibitors, to inaccessible tumour areas and thereby helping to prevent tumour relapse.

Methods: We applied two different types of focused ultrasound sequences (long pulses vs rapid short-pulses) with microbubbles to the left hippocampus of wild-type female C57BL/6 mice before administering fluorescently labelled cytotoxic T lymphocyte-associated antigen-4 antibodies.

Results: We determined that the targeted brain region had a significant increase in antibody delivery following ultrasound treatment with both pulse sequences. A more uniform delivery was achieved when treating with rapid short-pulse sequences (*p-value* = 0.0130), where bursts of short 5 µs pulses of focused ultrasound were emitted at a fast repetition frequency (1.25 kHz). We observed a significant increase in anti-tumour immune cells in long-pulse treated brains (*p-value* = 0.0021 ($CD3^+$ cells) and *p-value* = 0.0001 (MHC class II^+ cells)).

Conclusion: These results provide a proof-of-principle for how focused ultrasound with microbubbles can promote homogenous anti-tumour drug delivery and modulate the immune microenvironment.

Keywords: focused ultrasound, blood-brain barrier, microbubbles, drug delivery, immunotherapy, immune checkpoint inhibitors

Introduction

Gliomas are the most common malignant tumours in the adult central nervous system (CNS) with glioblastoma being their most aggressive form.[1,2] Currently available treatments include surgery to resect the tumour, chemotherapy and radiotherapy.[3] Despite these treatment strategies, the prognosis of gliomas, and in particular glioblastomas, remains poor, with median survival following diagnosis of approximately 12–18 months.[3] The main hindrance to an effective treatment strategy lies in tumour heterogeneity, as glioblastomas are made up of different subtypes of glioma stem cells that react differently to treatments.[4] There is therefore a need for a treatment strategy that addresses the heterogeneity of glioma's cellular make-up. In other words, we need a treatment strategy that globally targets different elements of the tumour microenvironment, including the tumour cells, immune cells, cytokines and endothelial cells that are found in gliomas.[2]

Immune checkpoint blockers represent an emerging treatment strategy that acts to block the pro-tumour effects of immune checkpoints, proteins that are over-expressed on the surface of T cells, particularly $CD4^+$ and $CD8^+$ T cells, in the tumour microenvironment.[5] Figure 1 highlights the mechanism of action of one such type of immune checkpoint,

https://doi.org/10.2147/ITT.S569804
Received: 8 October 2025
Accepted: 7 January 2026
Published: 2 February 2026

Graphical Abstract

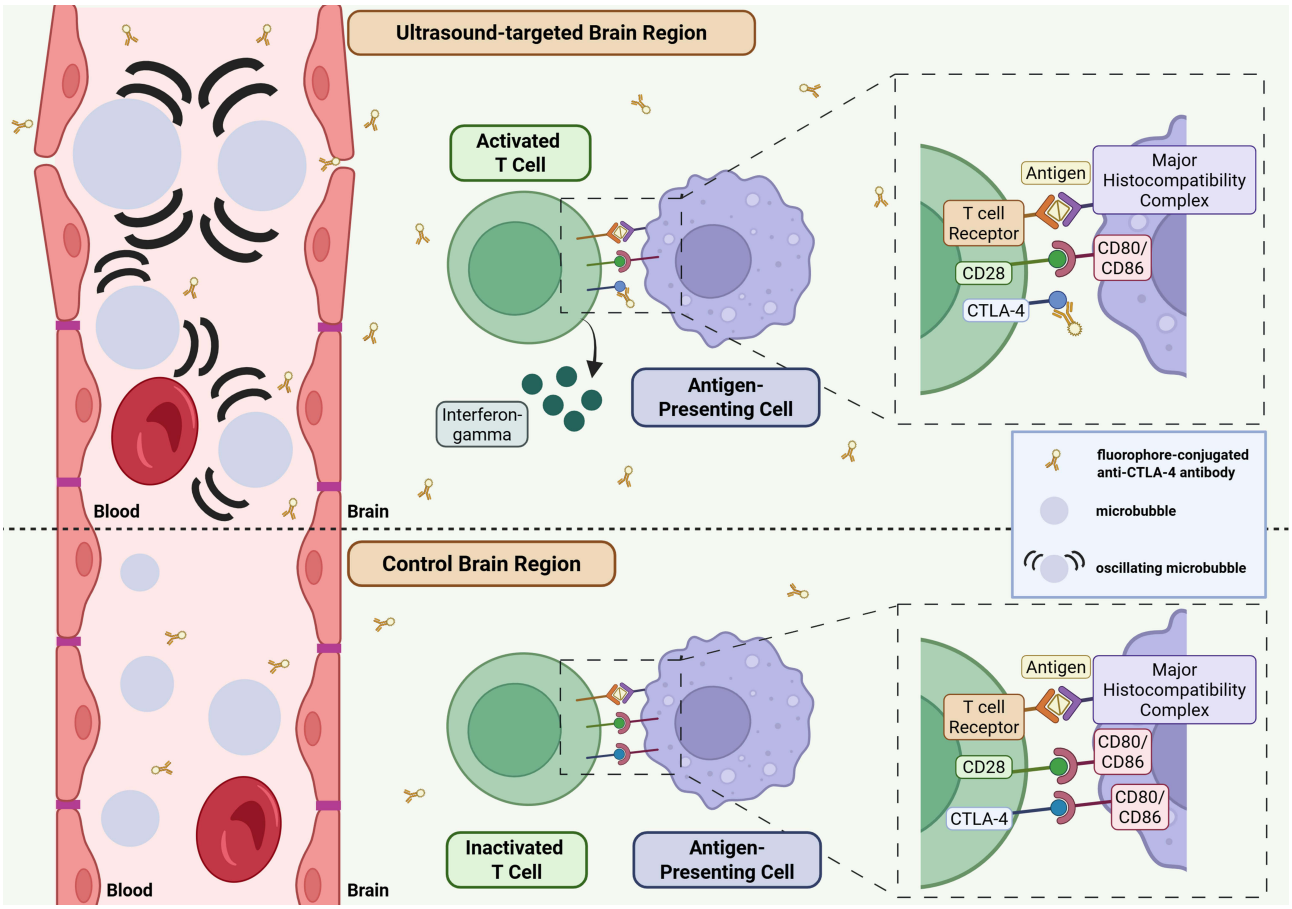

cytotoxic T lymphocyte-associated antigen-4 (CTLA-4), which, when not blocked by an anti-CTLA-4 antibody (immune checkpoint inhibitor), binds to receptors on antigen-presenting cells (APCs), promoting the inactivation of T cells (Figure 1A).[5] Research has been carried out to determine the effectiveness of these immune checkpoint blockers. For example, Chen et al demonstrated that anti-CTLA-4 treatments led to a 2- to 3-fold increase in survival in a glioma mouse model enriched with mesenchymal-like glioma stem cells, the most aggressive subtype of glioma stem cells, making it more representative of human glioblastomas compared to commercial glioma mouse models.[4] This method of immune suppression is crucial for glioma survival as $CD4^+$ and $CD8^+$ T cells normally play key anti-tumour roles in the tumour microenvironment by secreting pro-inflammatory cytokines such as interferon-gamma (IFN-γ) to recruit more T cells.[2] The activation of these T cells is dependent on their interaction with APCs, which include dendritic cells, B cells and microglia.[6] In fact, in tumours where the function of dendritic cells is impaired, T cell activity is lower as both $CD4^+$ and $CD8^+$ T cells lose their ability to react to antigens.[6] Therefore, immune checkpoint blockers are a promising treatment strategy as they can counteract key pro-tumour mechanisms of gliomas, such as the overexpression of immune checkpoints, to promote T cell activation. The delivery of these antibodies to the brain, however, is hindered by the impermeability of the blood-brain barrier (BBB).[4]

The BBB is responsible for maintaining homeostasis in the CNS and protecting it against toxins and pathogens.[7] This is made possible by the presence of junction proteins between the endothelial cells that line the capillary walls, which also contain efflux pumps, rendering the brain impermeable to most large-molecule drugs.[7] In tumours, however, the BBB is leaky in a heterogeneous way and is most commonly referred to as the blood-tumour barrier (BTB).[8] This means

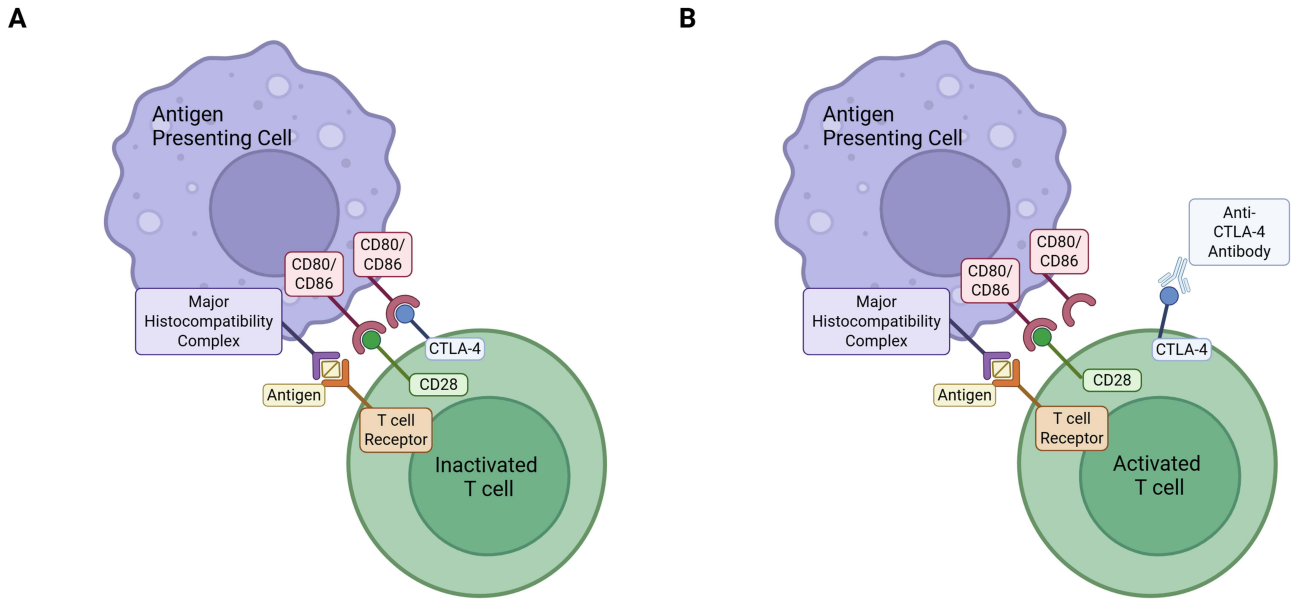

Figure 1 *Immune checkpoint inhibition*. T cell activation requires antigen presentation by antigen-presenting cells (APCs) via the major histocompatibility (MHC)-T cell receptor (TCR) complex along with the binding of CD28 with the CD80/CD86 receptor on APCs. If the CTLA-4 protein is upregulated (**A**), it will interact with the CD80/CD86 receptor on the surface of APCs and cause T cells to become inactive. However, if an anti-CTLA-4 antibody is present (**B**), it will interact with the CTLA-4 protein and prevent its interaction with the CD80/CD86 receptor, allowing T cell activation. This figure was created using BioRender and adapted from the National Cancer Institute.[5]

that regions within the tumour that need to be targeted for an effective anti-tumour response will experience varying degrees of drug delivery, which in turn can promote tumour recurrence.[8]

Focused ultrasound (FUS) with microbubbles (MBs), a technique first described in 2001 by Hynynen et al, can promote a safe, reversible, and targeted increase in the permeability of the BBB.[9] This technology focuses ultrasound waves onto targeted regions within the brain with MBs being administered into the bloodstream.[10] These MBs are clinically approved as ultrasound contrast agents and most often consist of a protein or lipid shell containing a gas core, with diameters between 1–10 μm.[11] When these MBs enter the area where the ultrasound is targeted, they expand and contract causing mechanical stresses on the blood vessel walls, which increases the permeability of the BBB.[12] This technique has previously been used to deliver immune checkpoint blockers, programmed cell death ligand 1 (PD-L1) and the programmed cell death protein 1 (PD-1), across the BBB.[13,14] Both studies showed an increase in the delivery of these antibodies to the brain with FUS, emitted in sequences of long 10 ms pulses.[13–15] Here, we sought to investigate whether FUS and MBs could increase the delivery of anti-CTLA-4 immune checkpoint blockers to the brain, and whether a rapid short-pulse (RaSP) sequence could be used for this purpose. RaSP sequences, consisting of bursts of short microsecond pulses emitted at a fast repetition frequency, have been shown to promote a more homogeneous delivery of a variety of agents, with a higher safety profile and faster closing of the BBB.[15–19] In other words, RaSP has the potential to enable a more uniform, widespread delivery of anti-CTLA-4 antibodies, allowing them to reach more locations where the BTB is still intact. Improving the uniformity of drug delivery takes away the pressure from other methods to ensure drug delivery, such as increasing local drug concentrations by injecting more drug systemically, which has been shown to correlate (C_{min}) with an increase in immune-related adverse effects following administration of ipilimumab (commercial anti-CTLA-4 antibody).[20]

Healthy wild-type female C57BL/6 mice were used as a model of the most impermeable conditions for these antibodies to get across, given their intact BBB. We targeted the left hippocampus of the mouse's brain with either a long-pulse or RaSP ultrasound sequence while intravenously injecting MBs followed by a fluorophore-conjugated anti-CTLA-4 antibody. Once extracted, the brains were cryosectioned and imaged to quantify the amount of fluorescence detected in the targeted hippocampus compared to that in the control brain region (that received no ultrasound treatment)

https://doi.org/10.2147/ITT.S569804

to determine how long-pulse versus RaSP ultrasound treatments affected delivery. We then sought to explore whether these treatments modulated the immune microenvironment of the targeted brain region. To address this second aim we stained sections from the treated mice for cluster of differentiation 3+ ($CD3^+$) and major histocompatibility complex class II+ (MHC class II^+) cells. $CD3^+$ was used as a common marker for T cells, which play key roles in anti-tumour immunity and are the targets of anti-CTLA-4 antibodies. We stained for MHC class II^+ cells as these are the APCs for a subset of T cells, $CD4^+$ T cells, that trigger the cytotoxic $CD8^+$ T cell response and promote the formation of a memory $CD8^+$ T cell pool that is needed for long-term anti-tumour responses.[21]

Materials and Methods

Animals

Wild-type female C57BL/6 mice (Charles River, Stansted, UK) (N= 6) between 8–12 weeks old (19.82 ± 2.23 g) were used for these experiments that took place between September 2023 and September 2024. These mice were all habituated for at least seven days before any experiment and held in individually ventilated cages (inside temperature 20–24°C) and humidity-controlled rooms (45–64%) with 12-hour night and day cycles. These experiments were all approved by Imperial College London's Animal Welfare and Ethical Review Body and the UK Home Office regulatory establishments and performed following the UK Animals (Scientific Procedures) Act of 1986 (Licence number: PBDB8AA12). This study was conducted according to the ARRIVE guidelines.

Ultrasound Setup and Experimental Workflow

As described in previous work, mice were anaesthetized with 1.5–2.0% vaporized isoflurane (Zoetis UK Limited, London, UK) mixed with oxygen (1 L/min) using an anaesthesia vaporizer (Harvard Apparatus, Cambridge, UK) (Figure 2).[15,19] The fur on the top of the mouse's head was shaved using an electric trimmer and depilatory cream before the mouse was moved to the ultrasound setup and the head was fixed in place using a stereotaxic frame (45° ear bars; World Precision Instruments, Hertfordshire, UK). Gel was then applied to the top of the mouse's head onto which a water bath with a parafilm bottom was positioned. The targeting was then performed by placing a 1-mm-thick cross in the water bath in alignment with the lambdoid and sagittal sutures of the mouse's head. The left hippocampus was targeted, whilst the right hippocampus was used as a control, by positioning the ultrasound transducer 3 mm laterally from the sagittal suture, 0.5 mm anterior to the lambdoid suture and 3 mm inferior to the skull. A single-element spherical-segment focused ultrasound transducer (centre frequency: 1 MHz, focal depth: 60.5 mm, diameter: 90 mm; Sonic Concepts, Bothell, WA, USA) fitted inside a cone filled with distilled water and closed with a layer of parafilm was lowered into the water bath. For targeting, the transducer was connected to a pulser-receiver (DPR300; Insidix, Seyssins, France) and moved by a 3D computer-controlled positioning system (Velmex Inc., Bloomfield, NY, USA). For long-pulse ultrasound treatments, one function generator was used to emit a sequence of 10,000 cycle pulses at a pulse repetition frequency of 0.5 Hz. When emitting a RaSP sequence, two function generators were used for the pulse shape and pulse sequence (33500B Series; Agilent Technologies, Santa Clara, CA, USA). A sequence of 5 cycle pulses was emitted at a pulse repetition frequency of 1.25 kHz, grouped into 10 ms bursts repeated at a burst repetition frequency of 0.5 Hz. For both sequences, a derated peak negative pressure of 0.71 MPa was used and a total of 126 pulses were emitted. This pressure was chosen to ensure the extravasation of antibodies into the brain, given that our previous work has shown that 0.35 MPa is not sufficient for endogenous immunoglobulins to cross the blood-brain barrier.[15] The signal from the function generators was amplified with a 50-dB power amplifier (Precision Acoustics Ltd., Dorchester, UK). The pressure reported above is derated, considering an 11.2 ± 0.29% attenuation through the mouse's skull's parietal bone as reported previously.[19]

Following the emission of 5 control pulses of ultrasound, SonoVue® MBs (concentration: 5 µL/g of body mass, vial concentration: 3 × 108/mL, Bracco, Milan, Italy) were intravenously injected using a 30G catheter across a duration of 60 seconds. Immediately after, 5 µg PE/Cyanine7 anti-CD152 (clone: UC10-4B9, #106313, Biolegend, CA, USA) was injected intravenously through the tail vein. At the end of the ultrasound treatment, the mice immediately received an intraperitoneal injection of sodium pentobarbital (concentration: 200 mg/mL; volume: 0.01 mL/g; obtained from

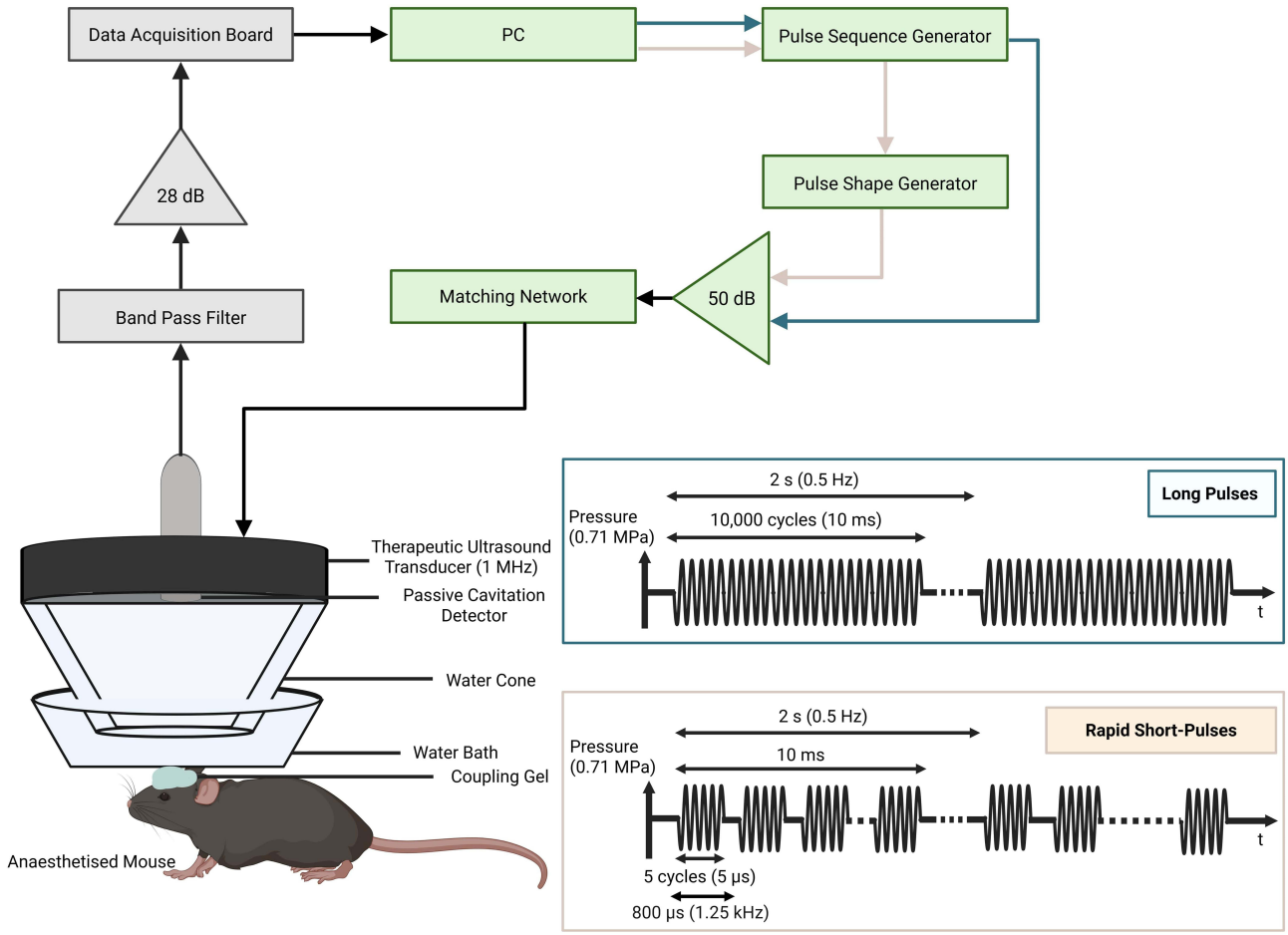

Figure 2 *Ultrasound setup*. Diagram showing one (for long-pulses) or two (for RaSP) function generators driving a 1 MHz transducer through an amplifier and a matching network. The transducer is fitted inside a sealed water cone that is lowered into a water bath positioned, using gel, on top of the mouse's head. The parameters of each of these two sequences and their respective sequence patterns are also shown. Long 10 ms pulses were emitted at a 0.5 Hz pulse repetition frequency, while 10 ms bursts of rapid short-pulses (RaSP) repeated at a 0.5 Hz burst repetition frequency were made up of short 5 cycle (5 µs) pulses emitted at a 1.25 kHz pulse repetition frequency. This figure was created using BioRender and adapted from Morse et al.[19]

Animalcare, UK) which was succeeded by a transcardial perfusion with ice-cold PBS (#18912-014, Sigma Aldrich, St Louis, MO, USA) followed by 10% formalin (Sigma Aldrich, St Louis, MO, USA). Brains were extracted and fixed in 10% formalin for 24 hours and then cryopreserved in 30% sucrose (#S/8600/53, Thermo Fisher, Waltham, MA, USA) dissolved in dH_2O until sectioning.

Sectioning

Brains were embedded in OCT (Agar Scientific, Stansted, UK) using an isopentane (#126470010, Thermo Fisher, Waltham, MA, USA) and dry ice bath. We then cryosectioned 30 µm horizontal brain sections using a CryoStar NX70 (Thermo Fisher, Waltham, MA, USA) cryostat with a chuck holder temperature of −16°C and a blade temperature of −18°C. The sections were then transferred onto Superfrost Plus™ Microscope Slides (#631–0108, VWR, Radnor, PA, USA) and imaged within two days using a Zeiss Axio Observer microscope (Oberkochen, Germany).

Immunofluorescence Staining Workflow

T cells were stained using a rat anti-mouse CD3 primary antibody (1:200; clone: KT3, #MCA500G, Bio-Rad, CA, USA) with 1% (w/v) milk powder (Tesco, Hertfordshire, England) dissolved in TBS (#524750-1EA, EMD Millipore Corporation, Burlington, MA, USA) and a secondary Alexa Fluor 488 goat anti-rat IgG H&L secondary antibody (1:400; #ab150157, Abcam, Cambridge, England) with 1% (w/v) milk powder in TBS. MHC class II^+ cells were stained

https://doi.org/10.2147/ITT.S569804

using a primary anti-rat MHC class II (I-A/I-E) purified antibody (1:100; clone: M5/114.15.2, #15227417, Thermo Fisher, Waltham, MA, USA) with 0.1% Triton-X (Sigma Aldrich, St Louis, MO, USA) and 1% bovine serum albumin (#A4378-5G, Sigma, St Louis, MO, USA) in PBS and a secondary Alexa Fluor 488 goat anti-rat IgG H&L antibody (1:500; #ab150157, Abcam, Cambridge, England) with 0.1% Triton-X and 1% bovine serum albumin in PBS.

Staining was performed by first allowing microscope slides to air dry for 10 minutes. Antigen retrieval was then performed using citrate buffer (1x; #C9999, Sigma Aldrich, St Louis, MO, USA) diluted in dH_20 at 80°C for either 1 minute (MHC class II^+ cells) or 10 minutes ($CD3^+$ cells) followed by a cooling period of 10 minutes. The slides were then permeabilised in either 0.1% Triton-X dissolved in PBS (MHC class II^+ cells) or 0.5% Triton-X dissolved in TBS ($CD3^+$ cells) for 30 minutes at room temperature on a shaker at 120 rpm. This was followed by a blocking period of 1 hour in 5% normal goat serum (#ab7481, Abcam, Cambridge, England) diluted in PBS (MHC class II^+ cells) or TBS ($CD3^+$ cells) on the shaker at 120 rpm at room temperature followed by an overnight incubation at 4°C in the primary antibody solution mentioned above. This was then followed by a 2-hour incubation with a secondary antibody (mentioned above) at room temperature on the shaker at 120 rpm followed by a fluoroshield mounting media with DAPI (#ab104139, Abcam, Cambridge, England) counterstain incubation for 2 minutes. The slides were then covered with a coverslip and sealed with nail polish and, after a day of air drying, were imaged on the Zeiss Axio Observer microscope.

Imaging

All imaging was performed on the Zeiss Axio Observer microscope (Oberkochen, Germany), using the 10x/0.3 Ph1 EC Plan-Neofluar (FWD = 5.2mm) objective. PE/Cyanine7 fluorophore was excited at 550/25 nm with emissions filtered at 605/70 nm. DAPI was excited at 390/40 nm with emissions filtered at 450/40 nm, and Alexa Fluor 488 was excited at 470/40 nm with emissions filtered at 525/50 nm.

Image Analysis

To compare delivery between long-pulse and RaSP sequences, we used the normalised optical density (NOD) measurement.[19] First, images were normalised by using MATLAB R2024a (Mathworks, Natick, MA, USA) to adjust the histogram of individual pixel intensity distribution of each image to match that of a reference image, also known as the histogram transfer method of normalisation. To calculate the NOD, we first subtracted individual pixel intensities from the treated and control regions of interest (ROIs), which are consistently sized areas from the sonicated/control brain regions selected for analysis, from the mean pixel intensity of the control ROI. We then summed the intensities with successful delivery, which was set to twice the standard deviation of the control ROI mean intensity, as shown in previous publications.[15,19,22–24] The NOD for each section was then calculated by subtracting the summed intensities that represented successful delivery of the control ROI from the target ROI. The NOD for each biological replicate was then determined by taking the average of individual NODs of each section across a brain thickness of 810 μm.

To determine the distribution of delivery, the coefficient of variation (COV) was calculated for each brain by determining the average ratio of standard deviation to the mean of the pixel intensity in the targeted ROI for each biological replicate across a brain thickness of 810 μm.

To quantify the number of immune cells in the targeted ROI compared to the control ROI, we used an automated pipeline designed in CellProfiler (Broad Institute, MA, USA). For all immune cells, the pipeline was designed to first select appropriate channels showcasing cell staining and convert these images to grayscale images. Any uneven illumination across the images was corrected, the background was reduced, and a function was then applied to enhance the cells of interest before identifying them based on their diameter and automatically counting them. This process was applied to 30 μm sections across a brain thickness of 270 μm. The raw data used to calculate the NOD, COV and immune cell counts was generated in a blinded manner towards the type of ultrasound sequence (long-pulse or RaSP) each brain section received.

Statistical Analysis

A two-tailed unpaired *t*-test with Welch's correction with a 95% confidence level was carried out for the NOD data (long-pulse vs RaSP), to account for unequal variances between groups (*F*-test to compare variances: $F = 84.57$, *p-value* = 0.0234) seeing as the data is likely normally distributed as determined by the Shapiro–Wilk normality test (*p-value* > 0.5). A two-tailed unpaired *t*-test with a 95% confidence level was carried out for the COV data (long-pulse vs RaSP), to account for unequal variances between groups (*F*-test to compare variances: $F = 4.980$, *p-value* = 0.3345) seeing as the data was normally distributed. For the $CD3^+$ and MHC class II^+ cell count analysis, unpaired multiple t-tests with Welch's correction (as we could not assume equal variances between the two groups) were carried out with the false discovery rate approach to correct for multiple comparisons as the data is likely normally distributed as determined by the Shapiro–Wilk normality test (*p-value* > 0.5). Multiple t-testing was used to compare the differences between treated and control brain regions ($CD3^+$ cell count: long-pulse (*p-value* = 0.0021, q-value = 0.0021), RaSP (*p-value* = 0.1219, q-value = 0.0616); MHC class II^+ cell count: long-pulse (*p-value* = 0.0001, q-value = 0.0001), RaSP (*p-value* = 0.0918, q-value = 0.0463)). Data in graphs is shown as mean ± SEM.

All statistical analyses were performed with GraphPad Prism 10 (Dotmatics, MA, USA). All p-values below 0.05 were determined to be statistically significant. Outliers for each calculation were determined using the interquartile range (IQR) method, with values excluded if they were larger than the sum of the third quartile and 1.5 times the IQR or lower than the first quartile minus 1.5 times the IQR.

Results

RaSP Ultrasound Promotes a Homogeneous Delivery of Anti-CTLA-4 Antibodies to the Brain

Following FUS treatment to the left hippocampus, we observed an increase in the detected fluorescence in the targeted brain region, indicating delivery of the fluorophore-conjugated anti-CTLA-4 antibody, compared to the control region, regardless of the ultrasound parameters used (Figure 3A–3D).

To quantify the difference in successful delivery between the two ultrasound sequences, RaSP and long-pulses, we measured the intensity across all imaged sections by calculating the NOD (Figure 3E). This measurement showed that there was no significant difference (*p-value* = 0.1095) in the NOD between long-pulse and RaSP-treated mice at an ultrasound pressure of 0.71 MPa (centre frequency = 1 MHz), meaning no significant differences were observed in the amount of anti-CTLA-4 antibody delivered between these two sequences. A larger range (122,683 compared to 13,293) and standard error (± 35,668 compared to ± 3,879) of NOD was observed in long-pulse compared to RaSP-treated brains. Furthermore, we determined the heterogeneity of delivery between these two parameters using the COV calculation to be significantly decreased (*p-value* = 0.0130) in RaSP (0.0037 ± 0.00093) compared to long-pulse-treated brains (0.0134 ± 0.0021), indicating a higher uniformity in delivery with RaSP (Figure 3F).

Ultrasound with Microbubbles Also Modulates the Immune Microenvironment

Changes to the immune microenvironment following ultrasound treatment were determined with immunofluorescence staining to detect the presence of T cells and MHC class II^+ cells. Co-localisation between the anti-CTLA-4 antibody and $CD3^+$ T cells was observed as well as proximity between the anti-CTLA-4 antibody and MHC class II^+ cells regardless of the ultrasound sequence used (Figure 4A–4D).

We then studied the difference in the number of immune cells in the sonicated brain region compared to that of control brain regions (Figure 5A–5H). In long-pulse-treated brains, more immune cells were detected in the targeted brain regions compared to the control regions when staining for $CD3^+$ and MHC class II^+ cells (Figure 5A, 5B, 5E and 5F). In RaSP-treated brains (Figure 5C, 5D, 5G and 5H) an observable difference between the number of both types of immune cells was observed in the treated brain region compared to the control brain region. However, less cells were detected in the RaSP-treated brains compared with long-pulses. We quantified these observations by determining the total cell count of each of these types of immune cells present in the treated brain region compared to control regions for both ultrasound sequences (Figure 5I and 5J). This quantification showed that a significant

https://doi.org/10.2147/ITT.S569804

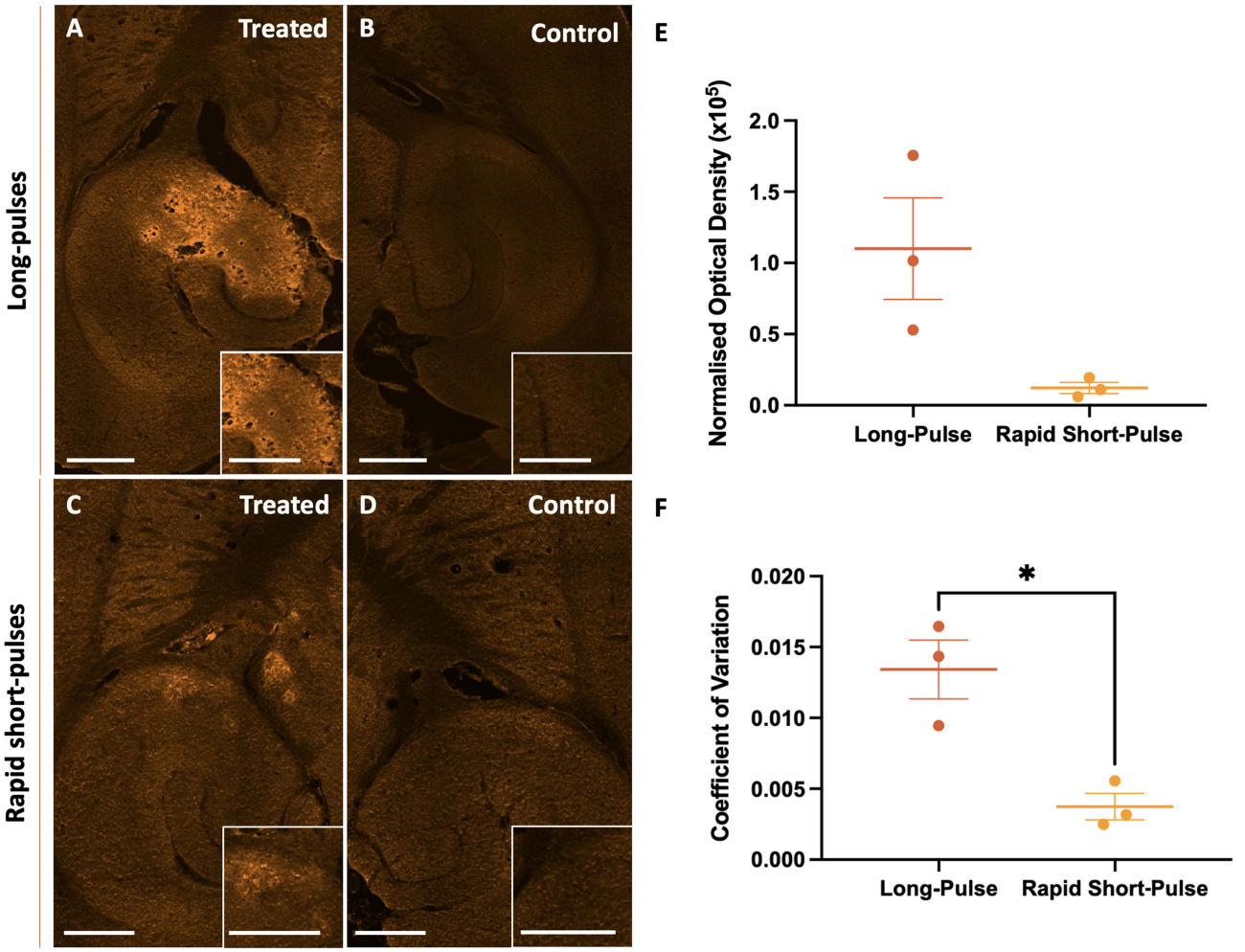

Figure 3 *Comparison of anti-CTLA-4 delivery following treatment with rapid short-pulses (RaSP) or long-pulses of focused ultrasound with microbubbles*. (**A**–**D**) Images showing the delivery, at higher magnification in the insets in the bottom-right corner of each panel, of fluorescently labelled anti-CTLA-4 in the ultrasound-treated brain regions (**A** and **C**) following long pulse (**A** and **B**) or RaSP (**C** and **D**) sequences emitted at a pressure of 0.71 MPa, with control brain regions (**B** and **D**). (**E**) Normalised optical density (NOD) quantification of the anti-CTLA-4 antibody delivery showed no significant difference in delivery between the two sequence types. (**F**) The distribution of the anti-CTLA-4 antibody within the targeted brain region was quantified using the coefficient of variation (COV), which shows a more homogeneous distribution following RaSP ultrasound treatment compared to long-pulses of ultrasound. Scale bars represent 500 µm. The plot shows mean ± SEM (n= 3); * *p-value* ≤ 0.05 (= 0.0130 (**F**)).

increase (*p-value* = 0.0021 for $CD3^+$ cells, *p-value* = 0.0001 for MHC class II^+) in the total count of $CD3^+$ cells and MHC class II^+ cells was present in the ultrasound-treated brain region compared to the control in long-pulse-treated mice.

Discussion

Regardless of the ultrasound pulse sequence applied, an increase in the delivery of anti-CTLA-4 antibodies was observed in the ultrasound-treated brain region compared to control regions in healthy wild-type mice (Figure 3A–3D). These results were expected given that the BBB is tendentially only permeable to lipophilic drugs smaller than 400–600 Da, and the anti-CTLA-4 antibodies administered, as IgG subtype antibodies, are approximately 150 kDa in molecular weight.[7,25] This antibody would, therefore, be too large to cross the BBB in areas where its permeability was not increased with FUS.

Having shown that FUS and MBs can increase the permeability of the BBB enough to allow anti-CTLA-4 antibodies to enter the brain, we were interested in comparing the differences in antibody delivery as well as changes in the immune microenvironment following treatments with sequences of either long-pulses or RaSP of ultrasound. The amount of

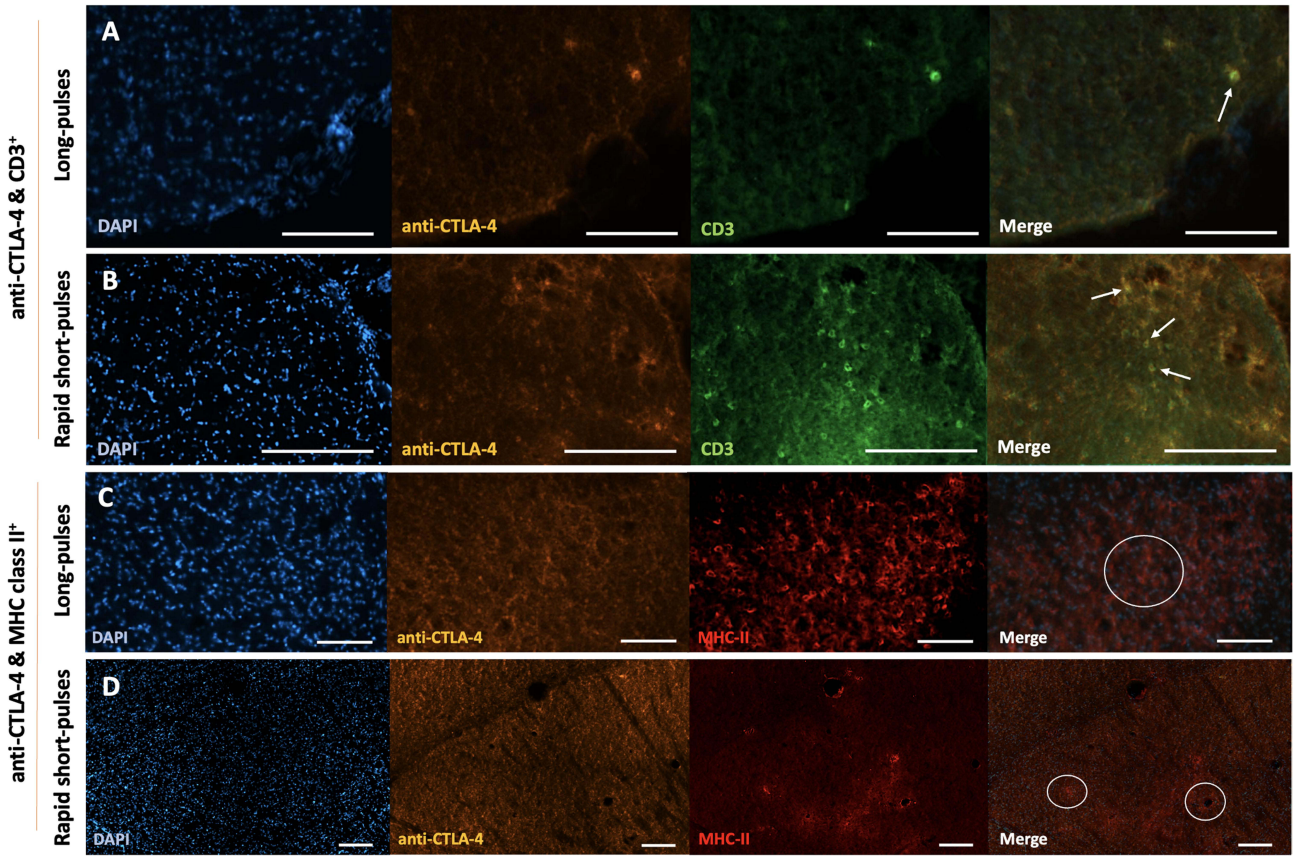

Figure 4 *Co-localisation of CD3$^+$ cells and MHC class II$^+$ cells with anti-CTLA-4 antibody.* (**A** and **B**) Immunofluorescence staining of CD3$^+$ cells in long-pulse ultrasound treated brains (**A**) and RaSP-treated brains (**B**) of wild-type mice superimposed with anti-CTLA-4 antibody fluorescence and DAPI (nuclei staining). (**C** and **D**) Immunofluorescence staining of MHC class II$^+$ cells in long-pulse (**C**) or RaSP-treated brains (**D**) of wild-type mice superimposed with anti-CTLA-4 antibody fluorescence and DAPI (nuclei staining).

Notes: Arrows are pointing to areas of CD3 and anti-CTLA-4 co-localisation. White circles highlight areas of anti-CTLA-4 antibody and MHC class II$^+$ cell proximity. Scale bars represent 100 µm (**A**–**C**) and 200 µm (**D**).

antibody delivery detected following long-pulse and RaSP treatments was not significantly different (Figure 3E), and the mice that underwent RaSP treatments showcased a lower COV (Figure 3F). Seeing as COV is a measure of the dispersion of the average fluorescence intensity compared to the mean, the fact that this value is lower in RaSP-treated brains indicates that there is less variation in the individual intensities in these mice, suggesting a more homogeneous distribution of the antibody. This can be explained by the nature of the RaSP sequence which is made up of short pulses repeated at a high repetition frequency. This sequence design is meant to allow more sustained MB activity and for them to travel along the vasculature in between pulses, promoting a more homogeneous opening of the barrier.[18] Long-pulse sequences, on the other hand, are characterised by longer pulses which are thought to stress specific locations along the blood vessels as the MBs oscillate for more cycles.[18] These observations are further reinforced by the fact that there was a higher range and standard error of the mean between the NODs of the three mice that were sonicated with long-pulses compared to the mice that were treated with RaSP, which suggests that there is a larger variability in the delivery following long-pulse treatments (Figure 3E). It is, however, important not to overinterpret this observation, considering the small sample size and, consequentially, the inherent variability between biological samples.

In terms of the immune microenvironment, a significant increase in the number of CD3$^+$ T cells and MHC class II$^+$ cells was observed both qualitatively and quantitatively only in long pulse-treated brains (Figure 5). However, instances of co-localisation between the anti-CTLA-4 antibody and these immune cells were observed in all treated mice independent of the sequence used (Figure 4). This co-localisation was expected given that both CTLA-4 and CD3 proteins are found on the surface of T cells, as CD3 proteins are part of the T cell receptor complex. MHC class II$^+$ cells

https://doi.org/10.2147/ITT.S569804

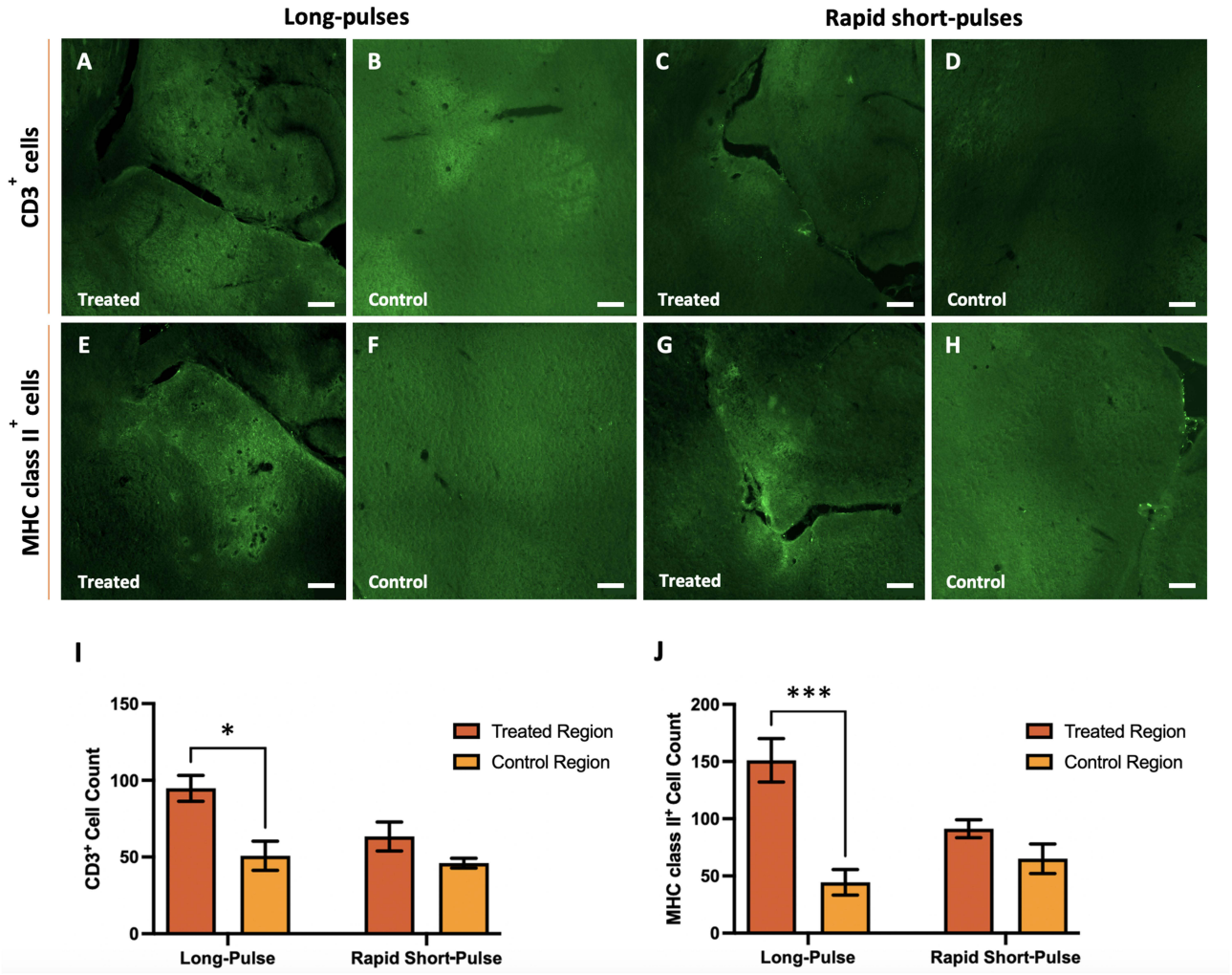

Figure 5 *$CD3^+$ and MHC class II^+ invasion in ultrasound-treated brain regions*. Immunofluorescence staining shows differences in the invasion of $CD3^+$ (**A–D**) and MHC class II^+ (**E–H**) cells into the ultrasound-treated brain regions (**A, C, E** and **G**) compared to control brain regions (**B, D, F** and **H**) using long-pulse (**A, B, E** and **F**) and RaSP (**C, D, G** and **H**) sequences. The total count of $CD3^+$ (**I**) and MHC class II^+ (**J**) cells was determined in treated brain regions targeted with ultrasound at 0.71 MPa with both long pulse and rapid short-pulse sequences compared to control (untreated) regions. A significant increase in T cells (**I**) and MHC class II^+ cells (**J**) was observed in ultrasound-treated compared to control brain regions in long-pulse treated brains. Scale bars represent 200 µm. The plot shows mean ± SEM (n= 3); **p-value* ≤ 0.05 (0.0021 (**I**)) and ****p-value* ≤ 0.0001 (0.0001 (**J**)).

are also responsible for antigen presentation to a sub-class of T cells which would bring them in close proximity to anti-CTLA-4 antibodies.[26,27]

A significant increase in the number of immune cells in the brain was only observed in long-pulse-treated brains, with a larger difference in fluorescence between treated and control brain regions for both immune cells being more prominent following long-pulse treatments compared to RaSP-treated brains (Figure 5A–5H). This effect was confirmed with quantitative analysis (Figure 5I–5J) and can be explained by the fact that, after ultrasound, higher levels of BBB leakage in mice treated with long-pulses were observed compared to those treated with RaSP (Figure 3A–3D). This is most likely due to long pulses of ultrasound leading to the permeability of the vasculature being increased more in some regions compared to others, compared to a more homogeneous opening with RaSP sequences. This increased extravasation could promote a higher number of T cells and, by extension, APC recruitment to targeted brain regions. This has been observed in patients who experience intracerebral haemorrhages, where these immune cells tend to migrate to the brain, and, particularly, T cells will converge onto areas of the vasculature where there is blood leakage or, in other words, a microhaemorrhage.[28] For this reason, since there was more extravasation with long-pulses, unsurprisingly, a larger number of T cells and MHC class II^+ cells were observed in these brains.

We would expect this trend to be maintained in the long-term considering that long-pulse sequences increase the permeability of the BBB for longer periods (between 4–48 hours) compared to RaSP sequences that have been shown to promote changes in BBB permeability for periods as low as 10–20 minutes with low acoustic pressures (0.35 MPa at 1 MHz).[18,19] This would mean more time for immune cells to infiltrate the brain following long-pulse treatments. Future work should explore these patterns in a glioma model to determine the specific roles and contributions of infiltrating/resident immune cells, following FUS treatment, to the tumour microenvironment.

These results show a significant increase in anti-CTLA-4 delivery when using FUS and MBs to increase the permeability of the BBB. Whilst treatment with RaSP sequences of ultrasound promotes a more homogeneous delivery of the antibody compared to long-pulse-treated mice, which would be advantageous considering the heterogeneous nature of the BTB, only long-pulse treatments influenced the immune microenvironment at this acoustic pressure. Future work is needed to fine-tune the parameters of these two sequences to find a "sweet spot" where we can promote both a homogeneous delivery of antibodies and stimulate crucial anti-tumour immune cells invasion. This could include, for example, increasing the acoustic pressure when emitting a RaSP sequence as this would promote a larger opening of the BBB and, consequently, more extravasation, as has been observed when delivering liposomes or endogenous immunoglobulins into the brain with RaSP.[15,18] Increasing the pulse length in the RaSP sequence could also be used as a way to further increase the permeability of the BBB. In addition, future studies should consider comparing these pulse sequences using a normalised acoustic dose. Considering the small sample size and animal model chosen for this study, this paper stands as an exploratory study that provides a proof-of-principal for the potential therapeutic use of FUS with MBs, particularly that of RaSP sequences, in improving immune checkpoint delivery for glioma treatment. Future work is needed to test whether these observations, particularly whether the changes in the immune microenvironment, would remain true in a larger cohort of mice and in a glioma mouse model.

Conclusion

We have therefore demonstrated how, by utilising different FUS sequences in tandem with MBs, we can achieve not only an increased delivery of immune checkpoint inhibitors but also modulate the immune microenvironment in a mouse model of the most impermeable BBB. This stands as a proof-of-principle for the potential of this treatment to ensure drug delivery to the most impermeable sections of the BTB and, consequentially, reduce the risk of tumour recurrence, increasing the likelihood of a successful treatment course in people with gliomas.

Data Sharing Statement

All the data from this paper can be provided upon request from the corresponding author.

Acknowledgments

We would like to thank the Facility for Imaging by Light Microscopy (FILM) at Imperial College London, part-supported by funding from the Wellcome Trust (grant 104931/Z/14/Z). Sophie V. Morse acknowledges funding from her Imperial College Research Fellowship.

Funding

Vanessa Drevenakova's graduate studies are supported by the Medical Research Council Doctoral Training Programme at Imperial College London [MR/W00710X/1]. Sophie V. Morse acknowledges funding from her Imperial College Research Fellowship. The Facility for Imaging by Light Microscopy (FILM) at Imperial College London is part-supported by funding from the Wellcome Trust (grant 104931/Z/14/Z) and BBSRC (grant BB/L015129/1).

Disclosure

The authors declare no competing interests in this work.

References

1. Pellerino A, Caccese M, Padovan M, Cerretti G, Lombardi G. Epidemiology, risk factors, and prognostic factors of gliomas. *Clin Transl Imaging*. 2022;10(5):467–475. doi:10.1007/s40336-022-00489-6

2. Chen H, Li M, Guo Y, et al. Immune response in glioma's microenvironment. *Innovative Surgical Sciences*. 2021;5(3–4):115–125. doi:10.1515/iss-2019-0001
3. Ipos D, Raposa BL, Freihat O, et al. Glioblastoma: clinical presentation, multidisciplinary management, and long-term outcomes. *Cancers (Basel)*. 2025;17(1):146. doi:10.3390/cancers17010146
4. Chen D, Varanasi SK, Hara T, et al. CTLA-4 blockade induces a microglia-Th1 cell partnership that stimulates microglia phagocytosis and anti-tumor function in glioblastoma. *Immunity*. 2023;56(9):2086–2104.e8. doi:10.1016/j.immuni.2023.07.015
5. National Cancer Institute. *Immune Checkpoint Inhibitors*. 2022.
6. Joiner JB, Pylayeva-Gupta Y, Dayton PA. Focused ultrasound for immunomodulation of the tumor microenvironment. *J Immunol*. 2020;205 (9):2327–2341. doi:10.4049/jimmunol.1901430
7. Wu D, Chen Q, Chen X, Han F, Chen Z, Wang Y. The blood–brain barrier: structure, regulation, and drug delivery. *Signal Transduct Target Ther*. 2023;8(1):217. doi:10.1038/s41392-023-01481-w
8. Gampa G, Vaidhyanathan S, Sarkaria JN, Elmquist WF. Drug delivery to melanoma brain metastases: can current challenges lead to new opportunities? *Pharmacol Res*. 2017;123:10–25. doi:10.1016/j.phrs.2017.06.008
9. Hynynen K, McDannold N, Natalia V, Jolesz FA. Noninvasive MR imaging–guided focal opening of the blood-brain barrier in rabbits. *Radiology*. 2001;220(3):640–646. doi:10.1148/radiol.2202001804
10. Chen KT, Wei KC, Liu HL. Focused ultrasound combined with microbubbles in central nervous system applications. *Pharmaceutics*. 2021;13 (7):1084. doi:10.3390/pharmaceutics13071084
11. Lee H, Kim H, Han H, et al. Microbubbles used for contrast enhanced ultrasound and theragnosis: a review of principles to applications. *Biomed Eng Lett*. 2017;7(2):59–69. doi:10.1007/s13534-017-0016-5
12. Chen S, Nazeri A, Baek H, et al. A review of bioeffects induced by focused ultrasound combined with microbubbles on the neurovascular unit. *J Cereb Blood Flow Metab*. 2022;42(1):3–26. doi:10.1177/0271678X211046129
13. Fadera S, Chukwu C, Stark AH, et al. Focused ultrasound-mediated delivery of anti-programmed cell death-ligand 1 antibody to the brain of a porcine model. *Pharmaceutics*. 2023;15(10):2479. doi:10.3390/pharmaceutics15102479
14. Lee H, Guo Y, Ross JL, Schoen S, Degertekin FL, Arvanitis C. Spatially targeted brain cancer immunotherapy with closed-loop controlled focused ultrasound and immune checkpoint blockade. *Sci Adv*. 2022;8(46):eadd2288. doi:10.1126/sciadv.add2288
15. W LKC, Chan TG, Raguseo F, et al. Rapid short-pulses of focused ultrasound and microbubbles deliver a range of agent sizes to the brain. *Sci Rep*. 2023;13(1):6963. doi:10.1038/s41598-023-33671-5
16. Morse SV, Rimer S, Geoghegan G, et al. Biological effects of rapid short pulses of focused ultrasound for drug delivery to the brain. *J Control Release*. 2025;382:113646. doi:10.1016/j.jconrel.2025.113646
17. Davies HJ, Morse SV, Copping MJ, et al. Imaging with therapeutic acoustic wavelets-short pulses enable acoustic localization when time of arrival is combined with delay and sum. *IEEE Trans Ultrason Ferroelectr Freq Control*. 2021;68(1):178–190. doi:10.1109/TUFFC.2020.3026165
18. Morse SV, Mishra A, Chan TG, de Rosales R, Choi JJ. Liposome delivery to the brain with rapid short-pulses of focused ultrasound and microbubbles. *J Control Release*. 2022;341:605–615. doi:10.1016/j.jconrel.2021.12.005
19. Morse SV, Pouliopoulos AN, Chan TG, et al. Rapid short-pulse ultrasound delivers drugs uniformly across the murine blood-brain barrier with negligible disruption. *Radiology*. 2019;291(2):459–466. doi:10.1148/radiol.2019181625
20. Le Louedec F, Leenhardt F, Marin C, Chatelut É, Evrard A, Ciccolini J. Cancer immunotherapy dosing: a pharmacokinetic/pharmacodynamic perspective. *Vaccines (Basel)*. 2020;8(4):632. doi:10.3390/vaccines8040632
21. Kilian M, Sheinin R, Tan CL, et al. MHC class II-restricted antigen presentation is required to prevent dysfunction of cytotoxic T cells by blood-borne myeloids in brain tumors. *Cancer Cell*. 2023;41(2):235–251.e9. doi:10.1016/j.ccell.2022.12.007
22. Morse SV, Boltersdorf T, Chan TG, Gavins FNE, Choi JJ, Long NJ. In vivo delivery of a fluorescent FPR2/ALX-targeted probe using focused ultrasound and microbubbles to image activated microglia. *Royal Soc Chem Chem Biol*. 2020;1(5):385–389.
23. Morse SV, Boltersdorf T, Harriss BI, et al. Neuron labeling with rhodamine-conjugated gd-based MRI contrast agents delivered to the brain via focused ultrasound. *Theranostics*. 2020;10(6):2659–2674. doi:10.7150/thno.42665
24. Chan TG, Morse SV, Copping MJ, Choi JJ, Vilar R. Targeted delivery of DNA-Au nanoparticles across the Blood–Brain barrier using focused ultrasound. *ChemMedChem*. 2018;13(13):1311–1314. doi:10.1002/cmdc.201800262
25. Charles A, Janeway J, Travers P, Walport M, Shlomchik MJ. The structure of a typical antibody molecule. In: *Immunobiology: The Immune System in Health and Disease*. 5th edn ed. Garland Science; 2001.
26. Kuhn C, Weiner HL. Therapeutic anti-Cd3 monoclonal antibodies: from bench to bedside. *Immunotherapy*. 2016;8(8):889–906. doi:10.2217/imt-2016-0049
27. Roche PA, Furuta K. The ins and outs of MHC class II-mediated antigen processing and presentation. *Nat Rev Immunol*. 2015;15(4):203–216. doi:10.1038/nri3818
28. Shi SX, Vodovoz SJ, Xiu Y, et al. T-lymphocyte interactions with the neurovascular unit: implications in intracerebral hemorrhage. *Cells*. 2022;11 (13):2011. doi:10.3390/cells11132011